Journal of Solid State Chemistry 184 (2011) 2159–2166

Contents lists available at ScienceDirect

Journal of Solid State Chemistry

journal homepage: www.elsevier.com/locate/jssc

Phase diagram, crystal chemistry and thermoelectric properties of compounds in the Ca–Co–Zn–O system

W. Wong-Ng [a,*], T. Luo [c], W. Xie [d], W.H. Tang [e], J.A. Kaduk [f], Q. Huang [b], Y. Yan [a], S. Chattopadhyay [f], X. Tang [g], T. Tritt [d]

[a] Ceramics Division, NIST, Gaithersburg, MD 20899, USA
[b] NIST Center for Neutron Research, USA
[c] Chemistry and Biochemistry Department, University of Maryland, MD 20745, USA
[d] Physics Dept., Clemson University, Clemson, SC 29631, USA
[e] Department of Physics, Zhejiang Sci-Tech University, Hangzhou 310018, China
[f] BCPS Dept., Illinois Institute of Technology, Chicago, IL 60616, USA
[g] Physics Department, Wuhan University, Wuhan 430070, China

ARTICLE INFO

Article history:
Received 29 March 2011
Received in revised form
10 June 2011
Accepted 13 June 2011
Available online 21 June 2011

Keywords:
Ca–Co–Zn–O phase equilibria
Structure of $Ca_3(Co_{1.95}Zn_{0.05})O_{6-z}$
Structure of $(Co_{2.7}Zn_{0.3})O_{4-z}$
Thermoelectric properties of
$Ca_3(CoZn)_4O_{9-z}$ and $Ca_3(CoZn)_2O_{6-z}$

ABSTRACT

In the Ca–Co–Zn–O system, we have determined the tie-line relationships and the thermoelectric properties, solid solution limits, and structures of two low-dimensional cobaltite series, $Ca_3(Co, Zn)_4O_{9-z}$ and $Ca_3(Co,Zn)_2O_{6-z}$ at 885 °C in air. In $Ca_3(Co,Zn)_4O_{9-z}$, which has a misfit layered structure, Zn was found to substitute in the Co site to a limit of $Ca_3(Co_{3.8}Zn_{0.2})O_{9-z}$. The compound $Ca_3(Co,Zn)_2O_{6-z}$ ($n=1$ member of the homologous series, $Ca_{n+2}(Co,Zn)_n(Co,Zn)'O_{3n+3-z}$) consists of one-dimensional parallel $(Co,Zn)_2O_6^{6-}$ chains that are built from successive alternating face-sharing $(Co,Zn)O_6$ trigonal prisms and 'n' units of $(Co,Zn)O_6$ octahedra along the hexagonal c-axis. Zn substitutes in the Co site of $Ca_3Co_2O_6$ to a small amount of approximately $Ca_3(Co_{1.95}Zn_{0.05})O_{6-z}$. In the ZnO–$CoO_z$ system, Zn substitutes in the tetrahedral Co site of Co_3O_4 to the maximum amount of $(Co_{2.49}Zn_{0.51})O_{4-z}$ and Co substitutes in the Zn site of ZnO to $(Zn_{0.94}Co_{0.06})O$. The crystal structures of $(Co_{2.7}Zn_{0.3})O_{4-z}$, $(Zn_{0.94}Co_{0.06})O$, and $Ca_3(Co_{1.95}\ Zn_{0.05})O_{6-z}$ are described. Despite the $Ca_3(Co, Zn)_2O_{6-z}$ series having reasonably high Seebeck coefficients and relatively low thermal conductivity, the electrical resistivity values of its members are too high to achieve high figure of merit, ZT.

1. Introduction

Over the last decade, the increase in global interest in research and development on thermoelectric (TE) materials has been partly due to the soaring short-term demand for energy and partly due to the need to create a sustainable energy future. The efficiency and performance of thermoelectric energy conversion is related to the dimensionless figure of merit (ZT) of the thermoelectric materials, given by $ZT=S^2\sigma T/\kappa$, where T is the absolute temperature, S is the Seebeck coefficient or thermoelectric power, σ is the electrical conductivity, and k is the thermal conductivity [1]. Only a small number of materials have been found to have practical industrial applications and they all have ZT values around or below 1.0. Optimization of the ZT values is not a straight-forward process because S, σ, and κ are interrelated. Recent reports that relatively high ZT values are possible in both thin film and bulk forms have revitalized interest in thermoelectric materials development [2–7].

The stability of metal oxides at high temperature has made these materials highly relevant to waste heat conversion applications. For example, the low-dimensional cobaltites that include $NaCoO_z$ [8], $Ca_2Co_3O_6$ [9,10], and $Ca_3Co_4O_9$ [11–14] exhibit the coexistence of large Seebeck coefficient and relatively low thermal conductivity. Consequently in recent years, considerable research has been conducted on oxides for thermoelectric applications.

Phase equilibrium diagrams provide road maps for processing and facilitating an understanding of material properties. Because of the promising properties of calcium-containing cobaltite, zinc-doped calcium cobaltites may also offer desirable properties. This paper discusses the phase compatibility relationships of the Ca–Co–O system, and crystal chemistry, crystallography, and thermoelectric property measurements of selected series of compounds in this system, including $Ca_3(Co, Zn)_4O_{9-z}$, and the $n=1$ Zn-doped homologous series, $Ca_{n+2}(Co,Zn)_n(Co,Zn)'O_{3n+3-z}$.

* Corresponding author
E-mail address: Winnie.wong-ng@nist.gov (W. Wong-Ng).

0022-4596/$ - see front matter © 2011 Elsevier Inc. All rights reserved.
doi:10.1016/j.jssc.2011.06.013

2. Experimental[1]

2.1. Sample preparation

Using high temperature solid-state synthesis techniques, 47 samples were prepared from stoichiometric amounts of $CaCO_3$, Co_3O_4, and ZnO (Table 1). These samples were mixed, pelletized, and annealed at 750 °C for one day, and subsequently annealed at 885 °C with intermediate grindings and pelletizations for another 7 days.

Powder X-ray diffraction was used to investigate the phase purity and establish phase relationships. These experiments were carried out using a Phillips X-ray powder diffractometer with Cu$K\alpha$ radiation and equipped with a series of Soller slits and a scintillation counter. The 2θ scanning range was from 10° to 80°, and the step interval was 0.03°. The ICDD PDF reference diffraction patterns of the Ca–Co–Zn–O systems [15] were used for performing phase identification.

For property measurements, the spark plasma sintering (SPS) technique was used for the preparation of high density pellets. The raw powder materials were consolidated into densified pellets at 1000 °C for 5 min under a pressure of 30 MPa. All samples have 90% or higher relative densities. The pellets were cut into bars of approximate dimensions of $2\,mm \times 2\,mm \times 10\,mm$ for the measurement of properties.

2.2. Structural studies using synchroton and neutron diffraction

2.2.1. Synchroton scattering studies

To study the structure of selected phases in the Ca–Co–Zn–O system (in particular, $Ca_3(Co_{1.95}Zn_{0.05})_2O_{6-z}$ and $(Zn_{0.98}Co_{0.02})O$), high resolution synchrotron powder diffraction data were collected using beamline 11-BM at the Advanced Photon Source (APS), Argonne National Laboratory, using an average wavelength of 0.412253 Å. Discrete detectors covering an angular range from 6° to 16° 2θ are scanned over a 34° 2θ range, with data points collected every 0.001° 2θ and a scan speed of 0.01°/s.

The 11-BM instrument uses X-ray optics with two platinum-striped mirrors and a double-crystal Si(111) monochromator, where the second crystal has an adjustable sagittal bend [16]. Ion chambers monitor incident flux. A vertical Huber 480 goniometer, equipped with a Heidenhain encoder, positions an analyzer system comprised of twelve perfect Si(111) analyzers and twelve Oxford-Danfysik $LaCl_3$ scintillators, with a spacing of 2° [17]. Analyzer orientation can be adjusted individually on two axes. A three-axis translation stage holds the sample mounting and allows it to be spun, typically at ≈ 5400 rpm (90 Hz). A Mitsubishi robotic arm is used to mount and dismount samples on the diffractometer [18].

The diffractometer is controlled via EPICS [19]. Data are collected while continually scanning the diffractometer 2θ arm. A mixture of NIST standard reference materials, Si (SRM 640c) and Al_2O_3 (SRM 676) [20] is used to calibrate the instrument, where the Si lattice constant determines the wavelength for each detector. Corrections are applied for detector sensitivity, 2θ offset, small differences in wavelength between detectors, and the source intensity, as noted by the ion chamber before merging the data into a single set of intensities evenly spaced in 2θ.

All data processing and structural refinements were carried out using the Rietveld refinement technique with the GSAS Suite [21,22]. In general, included in the refinements were the atomic coordinates, anisotropic metal displacement coefficients, isotropic oxygen displacement coefficients, a scale factor, and the lattice parameters. The peak profiles were described using a pseudo-Voigt function; the Gaussian U and W, the Cauchy X and anisotropic strain terms were refined. The backgrounds were described using a 6-term shifted Chebyshev polynomial.

X-ray powder reference patterns for samples in the Ca–Co–Zn–O system were obtained using a Rietveld pattern decomposition technique. These patterns represent ideal specimen patterns. They are corrected for systematic errors both in d-spacing and intensity. The reported peak positions are calculated from the refined lattice parameters, as this represents the best measure of the true positions.

2.2.2. Neutron diffraction studies

Neutron powder diffraction (NPD) data for $Zn_{0.3}Co_{2.7}O_{4-z}$ were collected at the NIST Center for Neutron Research on the high resolution powder neutron diffractometer (BT1), with monochromatic neutrons of wavelength 1.5403 Å produced by

Table 1
Samples prepared for the phase equilibria study of the Ca–Co–Zn–O system at 885 °C in air. The values given are the relative mol% of metallic components.

	Ca	Co	Zn
1	42.86	53.57	3.57
2	42.86	50.00	7.14
3	42.86	46.43	10.71
4	60	36	4
5	60	32	8
6	32.5	32.5	35
7	60	20	20
8	0	66.67	33.33
9	70	20	10
10	10	75	15
11	42.86	57	0.14
12	42.86	56.43	0.71
13	42.86	55.71	1.43
14	60	39.8	0.2
15	60	39	1
16	60	38	2
17	50	0	50
18	99.5	0	0.5
19	97.5	0	2.5
20	0.5	0	99.5
21	2.5	0	97.5
22	0	95	5
23	0	90	10
24	0	5	95
25	0	10	90
26	0	83.33	16.67
27	0	80	20
28	0	76.67	23.33
29	60	37	3
30	0	3	97
31	0	4	96
32	75	24	1
33	50	48	2
34	20	75	5
35	20	1	79
36	0	2	98
37	60	40	0
38	42.86	57.14	0
39	37	3	60
40	28	18	54
41	38	25	37
42	30	37.5	32.5
43	30	40	30
44	15	55	30
45	0	6.67	93.33
46	0	8.33	91.67
47	37.5	25	37.5

[1] The purpose of identifying the equipment in this article is to specify the experimental procedure. Such identification does not imply recommendation or endorsement by the National Institute of Standards and Technology.

a Cu(311) monochromator. Collimations before and after the monochromator and after the sample were 15′, 20′, and 7′ full-width-at-half-maximum (FWHM), respectively. Data were collected in the 2θ range of 3–168° with a step size of 0.05° at room temperature. Refinement of the nuclear structure was carried out using the neutron powder diffraction data and the Rietveld refinement technique using the software GSAS [21,22]. The neutron scattering amplitudes used in the refinements are 0.568, 0.253, and 0.581 for Zn, Co, and O, respectively.

2.2.3. EXAFS studies

EXAFS was used to evaluate the exact site substitution of Zn on the Co site in compounds where Zn substitution is only to a small extent. EXAFS measurements were performed on both Zn edge and Co edges of all the samples at the MRCAT 10-ID beamline located at the Advanced Photon Source in Argonne National Laboratory. Apart from the samples, we measured a solution of zinc nitrate in water (where zinc is 6-fold coordinated) [23]. ZnO powder was also measured since Zn in this compound is tetrahedrally bonded to oxygen atoms. With every EXAFS measurement, the zinc metal foil was measured as reference. The Zn edge of the sample of interest is placed along with Zn edges from Zn foil, ZnO powder, and $(Zn(NO_3)_2$ solution. The data were processed using Athena [24] and the data was modeled with Artemis [25] to find out the percentage of Zn atoms bonded tetrahedrally and octahedrally.

2.3. Thermoelectric property measurements

The thermal diffusivity was measured by the laser flash method using the Netzsch LFA457 system. Specific heat was determined by differential scanning calorimetry using a Netzsch DSC-404C. The density was calculated from the chemical formula and the unit cell volume. The resulting high temperature thermal conductivity, κ, was calculated from the measured thermal diffusivity, D, specific heat, C_P, and density, ρ_D, from the relationship: $\kappa = DC_P\rho_D$. The bulk materials were then cut into rectangular bars with the approximate dimensions of 2 mm × 2 mm × 10 mm. These bars were measured for electrical conductivity and Seebeck coefficient by a commercial ZEM-2 unit (Ulvac Riko, Inc.) under an inert gas (He) atmosphere from 300 to 900 K. Uncertainties in the electrical conductivity and thermal conductivity values are on the order of 5–7% due in large part in determination of the sample dimensions. The thermopower is known within about 2% and thermal diffusivity to within about 5%.

3. Results and discussion

Fig. 1 gives the phase diagram of the Ca–Co–Zn–O system that was determined at 885 °C in air. The phase relationships between solid solutions and other phases are expressed as tie-line bundles. The crystal chemistry, crystallography, and thermoelectric properties of various phases in the binary as well as the ternary oxide systems are discussed below.

3.1. CaO–ZnO system

No binary compound was found in the CaO–ZnO system. The literature reported that the $CaZnO_2$ phase was only successfully prepared under different processing conditions [15]. $CaZnO_2$ was also confirmed to be absent in a number of other reported systems such as the CaO–ZnO–SiO_2 [26] and CaO–ZnO–B_2O_3 [27] systems that were prepared in air.

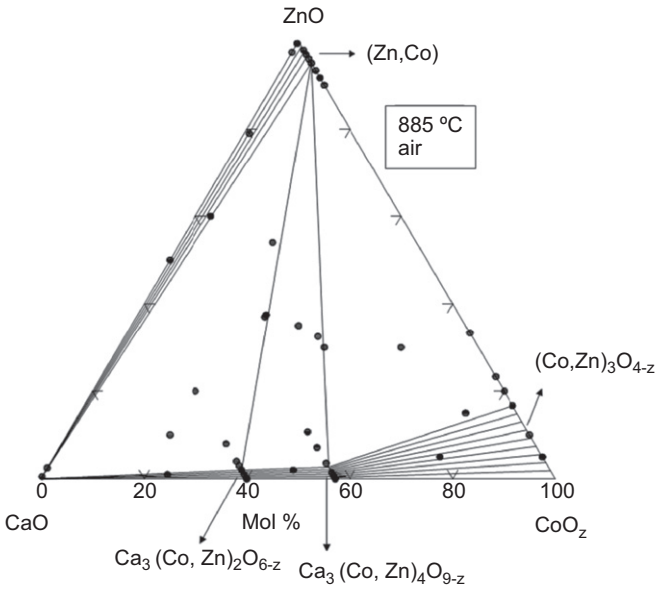

Fig. 1. Phase diagram of the CaO–CoO_z–ZnO system at 885 °C in air, showing the limits of various solid solutions, and the tie-line relationships of various phases.

3.2. CaO–CoO_z system

Two binary phases were determined in this system, namely, $Ca_3Co_2O_6$ and $Ca_3Co_4O_9$. The $Ca_3Co_4O_9$ phase has been extensively studied [28–32]. A very narrow solid solution region of $(Co,Ca)_3O_{4-x}$ was reported by Woermann and Muan [32] at around 890 °C. This region expands significantly at higher temperature. $Ca_3Co_4O_9$ is a misfit layered oxide that has two monoclinic subsystems with identical a, c, and β, but different b [29]. The first subsystem consists of triple rock-salt layers of Ca_2CoO_3 in the ab-plane while the second subsystem consists of a single CoO_2 layer, which has the CdI_2-type structure. This phase exhibits strong anisotropic thermoelectric properties in the ab-plane. It is thought that the increased scattering of phonons at the interface of misfit layers leads to the lowering of the lattice thermal conductivity. The chemical formula can be written as $[Ca_2CoO_3]RS[CoO_2]_{1.61}$, where RS is the rock salt and 1.61 expresses the incommensurable character for the b parameter of the rock salt and the CdI_2-type structure.

$Ca_3Co_2O_6$ ($R\bar{3}c$, $a=9.0793(7)$, and $c=10.381(1)$ Å [33]; Fig. 2) is the $n=1$ member of the homologous series with the general formula of $A_{n+2}B_nB'O_{3n+3}$. In this formula, A is an alkali-earth element such as Ca, Sr, and Ba [34], B describes the cobalt ion inside the octahedral cage, and B' is the cobalt ion inside a trigonal prism. $Ca_{n+2}Co_nCoO_{3n+3}$ consists of one-dimensional linear parallel $Co_2O_6^{6-}$ chains, built by successive alternating face-sharing CoO_6 trigonal prisms and CoO_6 octahedra along the hexagonal c-axis [35]. This face-sharing feature is in contrast to $Ca_3Co_4O_9$ [12] and $NaCo_2O_4$ [8], which consist of edge-sharing CoO_6 octahedra. The linear $Co_2O_6^{6-}$ chains of $Ca_3Co_2O_6$ consist of one CoO_6 octahedron alternating with one CoO_6 trigonal prism. These $Co_2O_6^{6-}$ chains are separated by octa-coordinated Ca^{2+} ions. The compounds $A_{n+2}Co_nCo'O_{3n+3}$ can also be considered as ordered intergrowth between the $n=\infty$ ($ACoO_3$) and $n=1$ ($A_3Co_2O_6$) end members [36,37]. We found that when A=Ca, only the $n=1$ member, namely, $Ca_3Co_2O_6$, can be made.

3.3. ZnO–CoO_x system

The only phases found in the ZnO–CoO_x system are the two solid solutions formed in the vicinity of ZnO and CoO_x. Co substitutes into

the Zn site of ZnO ($P6_3mc$, $a=3.250$ Å, $c=5.207$ Å [38]) to form $(Zn_{1-x}Co_x)O_{1-z}$ ($0<x\leq 0.06$)), and Zn substitutes into the tetrahedral Co site of Co_3O_4 ($Fd\bar{3}m$, $a=8.066(3)$ Å [39]) to form $(Co_{1-x}Zn_x)_3O_{4-z}$ ($0<x\leq 0.17$, with the maximum substitution composition of $(Co_{2.49}Zn_{0.51})O_{4-z}$). Apparently as temperature increases, the solid solution range of these two solid solutions increases as well. For example, it was reported that in the TiO_2–ZnO–CoO_z system [40], which was determined at 1050 °C in air, the solid solution limit of $(Zn_{1-x}Co_x)O_{1-z}$ was at a higher value of $x\approx 0.18$, and similarly, in $(Co_{3-x}Zn_x)O_{4-z}$, the limit was $x\approx 0.6$.

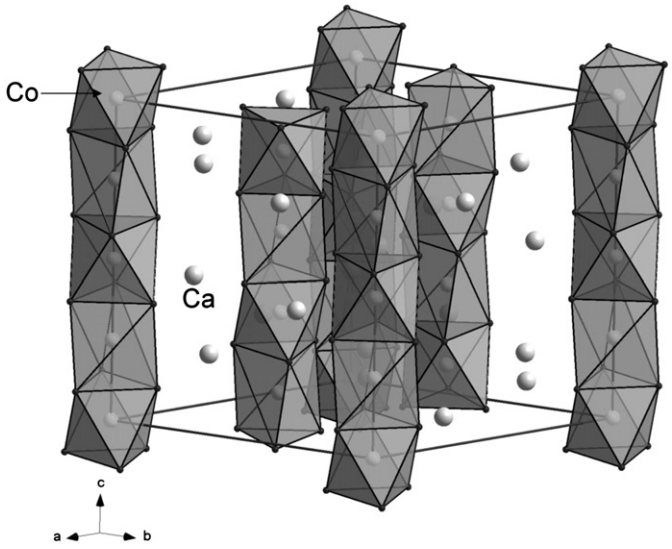

Fig. 2. Crystal structure of $Ca_3Co_2O_6$ ($n=1$ member in $Ca_{n+2}Co_nCoO_{3n+3}$), showing the feature of linear chains of successive alternations of CoO_6 octahedron with CoO_6 prism.

Table 2
Refined crystal structure of $(Zn_{0.98}Co_{0.02})O$; space group $P6_3mc$, $a=3.2505(1)$ Å, $c=5.2046$ (1) Å, and $V=47.623(1)$ Å^3.

Atom	x	y	z	Site occ.	U_{iso} (Å^2)	Mult
Zn1	1/3	2/3	0.0	0.98	0.02600(19)	2
Co2	1/3	2/3	0.0	0.02	0.02600(19)	2
O3	1/3	2/3	0.3828(4)	1.0	0.0270(7)	2

3.3.1. $(Zn_{1-x}Co_x)O$ ($x=0.02$)

This green-colored phase crystallizes in the hexagonal wurtzite type structure in which an extensive network of corner-shared ZnO_4 tetrahedra was found. Excellent Reitveld refinement results for $(Zn_{1-x}Co_x)O$ were obtained: $WR_p=0.0857$, $R_p=0.0675$, $\chi^2=3.391$, $R(F)=0.0280$, $R(F^2)=0.0586$. Table 2 gives the atomic coordinates and the distances. Essentially Co was found to dope in the Zn site. Fig. 3 gives the observed (crosses) and calculated (solid line) XRD intensities pattern at 295 K. The difference pattern is plotted at the same scale as the other patterns. The row of tick marks indicates the calculated peak positions. The refined Zn/Co site occupancy in the $(Zn_{1-x}Co_x)O$ phase is 0.98(2)/0.02. The refined space group and lattice parameters are $P6_3mc$, $a=3.2505(1)$ Å, $c=5.2046(1)$ Å, $V=47.623(1)$ Å^3, and $Z=2$. Fig. 4 gives the structure of $(Zn_{0.98}Co_{0.02})O$ projected along the c-axis. The metal–oxygen distances are 1.992(2) Å ($\times 1$) and 1.9733(6) Å

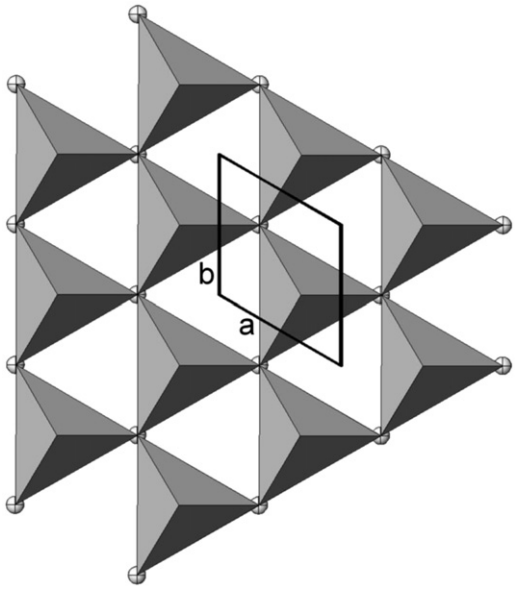

Fig. 4. Crystal structure of $(Zn_{0.98}Co_{0.02})O$ (of hexagonal wurtzite type).

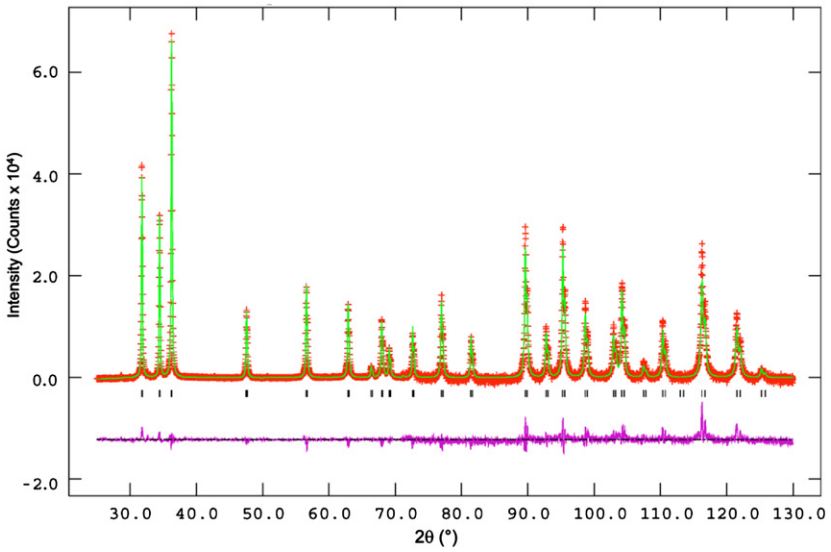

Fig. 3. Observed (crosses) and calculated (solid line) XRD intensities pattern for $(Zn_{0.98}Co_{0.02})O$ at 295 K.

(×3); the six O–(Zn,Co)–O bond angles are 108.01(6)° (×3) and 110.95(5)° (×3).

The pattern of Fig. 3 was collected on a Bruker D2 Phaser diffractometer equipped with a LynxEye position-sensitive detector using CuKα radiation at a tube power of 30 kV and 10 mA. The pattern was collected from 4.99782–130.004° 2θ in 0.0202144° steps, counting for 1 s/step.

3.3.2. Structure of $(Co_{1-x}Zn_x)_3O_{4-x}$ ($x=0.3$)

This black-colored phase has a cubic closed-packed spinel-structure. Fig. 5 gives the observed and calculated neutron powder diffraction intensities at room temperature. The refinement residues are: $WR_p=4.92\%$, $R_p=4.08\%$, and $\chi^2=1.148$.

In a normal AB_2O_4 spinel, A is a divalent atom and B is a trivalent atom. Table 3 gives the refined structure and atomic parameters for a selected representative composition of the normal spinel, $(Co_{2.7}Zn_{0.3})O_{4-z}$, at room temperature. $(Co_{2.7}Zn_{0.3})O_{4-z}$ is isostructural with Co_3O_4, which crystallizes in the space group of $Fd\bar{3}m$ ($a=8.08756(1)$ Å). In $(Co,Zn)_3O_{4-z}$, there are eight filled tetrahedral sites and 16 octahedral sites (8a and 16d) per unit cell. In one unit cell, there are 4 layers of BO_6 octahedral chains along the c-axis, with neighboring layers perpendicular to each other, as shown in Fig. 6. The CoO_4 tetrahedra are found between the CoO_6 octahedral chains (Fig. 7).

As the common coordination feature of Zn is tetrahedral, Zn was indeed found to substitute solely in the tetrahedral 8a site in the structure of $(Co_{2.7}Zn_{0.3})O_{4-z}$. The tetrahedral metal–oxygen distance in $(Co_{2.7}Zn_{0.3})O_{4-z}$ is 1.9434(3) Å (possibly of 2+ valence site), and the octahedral Co3–O5 distance is of an expected smaller magnitude of 1.9172(2) Å. It was reported that in a relatively highly doped spinel structure, $Co_{2.28}Cu_{0.72}O_4$ [41], Cu was found to substitute in both 8a and 16d sites of approximately equal quantities. Therefore it appears that when the dopant is of a small quantity, such as that in $(Co_{2.7}Zn_{0.3})O_{4-z}$, it will first enter the 8a site, and as the concentration of the dopant is increased, it would then enter the octahedral 16d site.

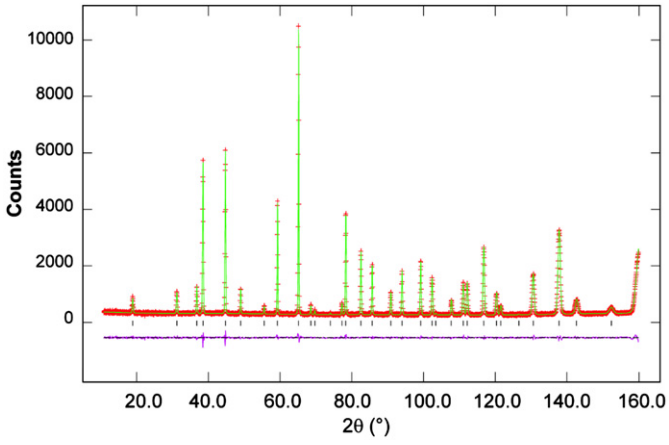

Fig. 5. Observed (crosses) and calculated (solid line) NPD intensities pattern for $(Co_{2.7}Zn_{0.3})O_{4-z}$ at 295 K.

Table 3
Refined structure and atomic parameters for $Zn_{0.3}Co_{2.7}O_{4-z}$ at room temperature using neutron diffraction (space group: $Fd\bar{3}m$, $a=8.08756(1)$ Å and $V=528.99(2)$ Å^3); $R_{wp}=4.92\%$ $R_p=4.08\%$, and $\chi^2=1.148$.

Atom	Frac	x	y	z	100 U_{iso}
Co(8a)	0.630(9)	1/8	1/8	1/8	0.47(5)
Zn(8a)	0.370(9)	1/8	1/8	1/8	0.47(5)
Co(16d)	1.000(6)	1/2	1/2	1/2	0.36(4)
Zn(16d)	0.000(6)	1/2	1/2	1/2	0.36(4)
O(32e)	0.990(2)	0.26374(2)	0.26374(2)	0.26374(2)	0.461(12)

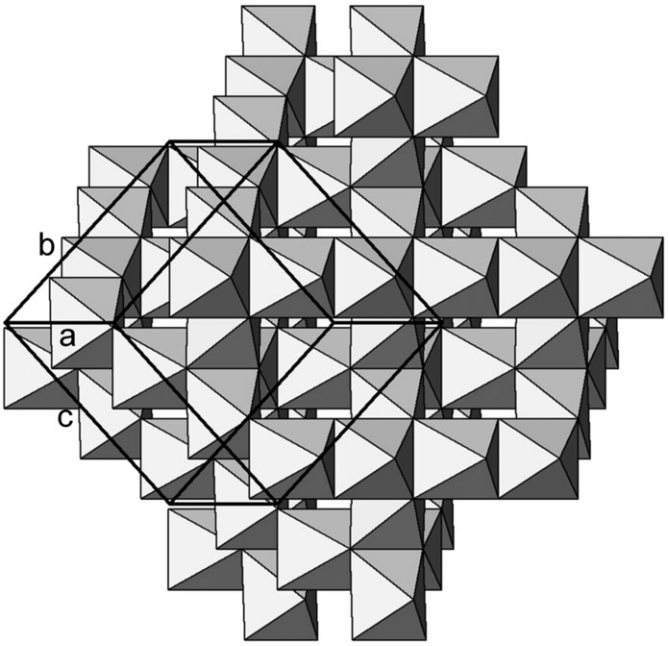

Fig. 6. Crystal structure of $(Co_{1-x}Zn_x)_3O_{4-z}$ showing neighboring octahedral layers perpendicular to each other.

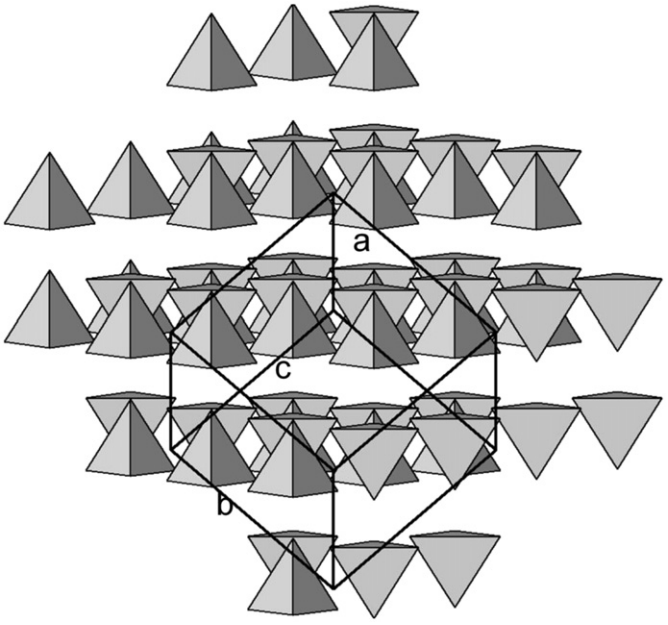

Fig. 7. Crystal structure of $(Co_{1-x}Zn_x)_3O_{4-z}$ showing the arrangement of the CoO_4 tetrahedra.

3.4. CaO–CoO_z–ZnO system

No new compound was found in the CaO–CoO_z–ZnO ternary system. Despite the report of a ternary Ca_3ZnCoO_{6-z} phase by Kawasaki and Takano [42], which is rhomobohedral, $R\bar{3}c$ ($a=9.09$ Å and $c=10.61$ Å) and crystallizes in the K_4CdCl_6 structure [43], this phase can only be prepared using the solution methods, followed by heat treatment under oxygen.

The tie-line relationships appear to be rather simple in the CaO–CoO_z–ZnO system. The limit of the two solid solution series, $Ca_3(Co,Zn)_2O_{6-z}$ and $Ca_3(Co,Zn)_4O_{9-z}$, are $Ca_3Co_{1.9}Zn_{0.1}O_{6-z}$ and $Ca_3(Co_{3.85}Zn_{0.15})O_{9-z}$. Tie-line bundles are found to be between $Ca_3(Co,Zn)_4O_{9-z}$ and $(Co,Zn)_3O_4$, between $Ca_3(Co,Zn)_2O_{6-z}$ and $Ca_3(Co,Zn)_4O_{9-z}$, and between $Ca_3(Co,Zn)_2O_{6-z}$ and CaO. The end members of the $Ca_3(Co,Zn)_2O_{6-z}$ and $Ca_3(Co,Zn)O_{4-z}$ series were found to be compatible with the $(Zn_{1-x}Co_x)O$ solid solution series.

The crystal structure of the $Ca_3(Co,Zn)_2O_{6-z}$ phase that was determined by X-ray Rietveld refinement technique can be described by Fig. 2. The structure consists of linear chains of face-sharing (Co, Zn)O_6 trigonal prisms and CoO_6 octahedra. Table 4 gives the refinement results, atomic coordinates and bond distances for $Ca_3(Co_{0.95}Zn_{0.05})_2O_{6-z}$. As reported in literature, the Zn–O tetrahedral bond is about 1.98 Å [44], and the Zn–O and Co–O octahedral bond lengths are at longer values of 2.083(3) and 2.0767(8) Å, respectively [45]. The prismatic Zn–O and Co–O bond distances are at further longer distances of 2.199(4) Å [46] and 2.018 Å [47], respectively. In the present structure, the average octahedral Co–O distance is 1.9111(5) Å, whereas the average Co–O prismatic distance is longer, 2.0713 (5) Å; therefore Zn most likely substitutes onto the prismatic Co–O site. However, as mentioned before, the X-ray diffraction technique is a technique for obtaining average Zn–O and Co–O bond distances and cannot conclusively provide the local structure information. The EXAFS results that provide local bonding environments are shown in Fig. 8. The white lines for the zinc nitrate and $Ca_3Co_{1.95}Zn_{0.05}O_{6-z}$ are almost at the same position, which is a signature of zinc being in 6-coordination state. The small pre-edge peak coincides with that of Zn in ZnO. This would suggest that Zn exists in a small amount in tetrahedral form (possibly in the amorphous form on the surface as a second phase). Zn has a small fraction residing in the tetrahedral site with a bond length 1.89 ± 0.05 Å and the main concentration is in the 6-coordination site with 2.11(2) Å (which is longer than the average octahedral Zn–O distance of 1.9111(5) Å). The 2.11(2) Å of Zn–O would suggest a bond length of a trigonal prism environment.

Table 4
Refined crystal structures of $Ca_3(Co_{1.95}Zn_{0.05})O_{6-z}$; space group $R\bar{3}c$ (lattice parameters, atomic coordinates, and bond distances).

a (Å)	9.07881(1)
c (Å)	10.39449(1)
V (Å^3)	741.979(1)
Ca1, x0¼	0.36898(2)
U_{11}	0.00528(7)
U_{22}	0.00555(10)
U_{33}	0.00371(10)
Co2/Zn3, 000	
frac	1/0
U_{11}	0.00281(8)
U_{33}	0.00132(13)
Co4/Zn5, 00¼	
frac	0.95/0.05
U_{11}	0.00638(8)
U_{33}	0.00232(14)
O6, x	0.17682(6)
y	0.02463(6)
x	0.11319(5)
U_{iso}	0.00530(12)
Ca1–O6 ×2 (Å)	2.3465(5)
×2 (Å)	2.4657(5)
×2 (Å)	2.5596(5)
×2 (Å)	2.4617(5)
Co2–O6 ×6 (Å)	1.9111(5)
O6–Co2–O6 (deg.)	86.07(2)
	93.93(2)
Co4–O6 ×6 (prismatic) (Å)	2.0713(5)
O6–Co4–O6 (deg.)	78.05(2)
	87.72(3)
	127.60(3)
	147.53(3)
R_{wp}	0.0975
R_p	0.0777
χ^2	2.133
$R(F)$	0.0339
$R(F^2)$	0.0426
$\Delta F+$	5.3
$\Delta F-$	−2.1
Profile coefficients	
U	2.33(4)
W	0.0655(5)
X	0.233(3)
ptec	−0.173
$S(400)$	0.00096(3)
$S(004)$	0.00358(4)
$S(202)$	0.00133(3)
Impurities	–

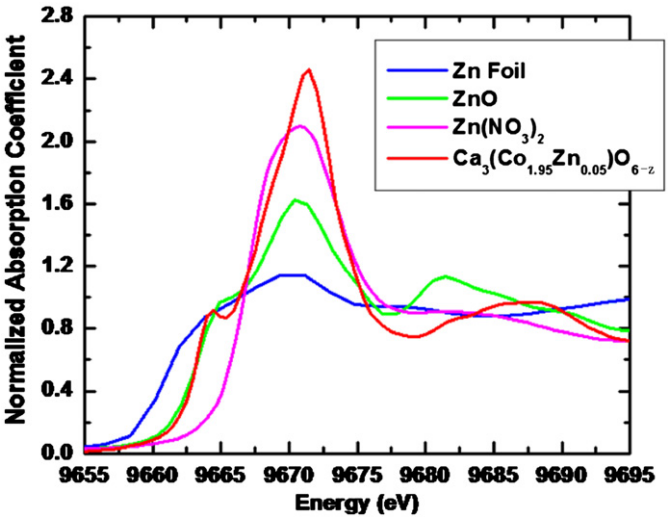

Fig. 8. EXFAS data for $Ca_3(Co_{0.95}Zn_{0.05})_2O_{6-z}$.

3.5. Thermoelectric properties

The thermoelectric properties of a number of compounds in the Ca–Co–Zn–O system have been reported in literature [33,48–55]. In the Ca–Co–O system, the $Ca_3Co_4O_9$ phase was reported to exhibit strong anisotropic properties and has excellent thermoelectric property in the *ab*-plane. *ZT* was reported to be ≈ 1 at 1000 K. It is thought that the increased scattering of phonons at the interface of misfit layers leads to the lowering of the lattice thermal conductivity. The Seebeck coefficient for single crystal $Ca_3Co_2O_6$ has been reported by Mikami and Funahashi [10] to be relatively high and positive, and the thermal conductivity is relatively low at high temperature. The transport properties are dominated mainly by p-type carriers. *ZT* was determined to be about 0.15 at 1000 K for a single crystal of $Ca_3Co_2O_6$.

The Seebeck coefficient, thermal conductivity, resistivity, and *ZT* values of $Ca_3Co_2O_6$, $Ca_3(Co, Zn)_2O_{6-z}$, $Ca_3(Co, Zn)_4O_{9-z}$, and $Ca_3(Co, Zn)_4O_{9-z}$ as a function of temperature, from this study, are given in Fig. 9a–d. The transport properties are dominated mainly by p-type carriers, with high temperature magnitudes between 200 μV/K at 900 K and 400–700 μV/K at 300 K for the

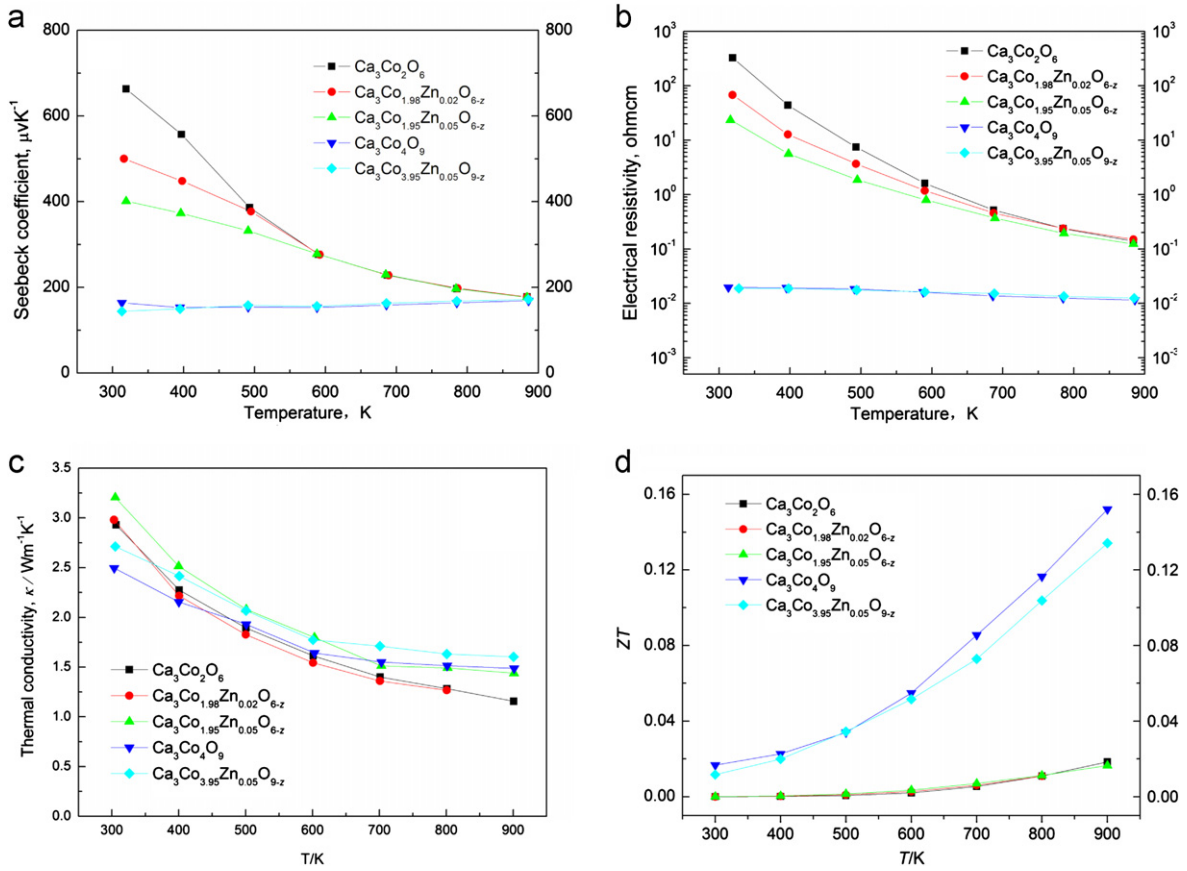

Fig. 9. (a) Seebeck coefficient, (b) resistivity, (c) thermal conductivity and (d) figure of merit, *ZT*, of $Ca_3Co_2O_6$, $Ca_3(Co, Zn)_2O_{6-z}$, $Ca_3Co_4O_9$, and $Ca_3(Co, Zn)_4O_{9-z}$ as a function of temperature.

$Ca_3(Co,Zn)_2O_{6-z}$ phase, and about 190 μV/K between 300 and 900 K for the $Ca_3(Co,Zn)_4O_{9-z}$ phase. The thermal conductivity data of the two solid solution series are similar and are reasonably low in the temperature range of 300–900 K. Zn substitution does not seem to have much effect on the thermoelectric properties of the $Ca_3(Co,Zn)_4O_{9-z}$ series. Although Zn-doping lowers the resistivity of the $Ca_3(Co,Zn)_2O_{6-z}$ series between 300 and 600 K, probably due to the changes of carrier concentration, at 900 K the values converge. The *ZT* value for our $Ca_3Co_4O_9$ sample (Fig. 9d) is not as high as reported [48], which is probably due to the fact that the processing conditions of our sample have not been optimized. The $Ca_3(Co,Zn)_4O_{9-z}$ series has a relatively higher *ZT* values than that of the $Ca_3(Co,Zn)_2O_{6-z}$ series. At present, the $Ca_3Co_4O_9$ compound remains the material that gives the highest *ZT* values among the oxides studied [48].

4. Summary

The phase diagram of the Ca–Co–Zn–O system that was determined at 885 °C in air provides detailed compatibility relationships in the binary and the ternary oxide systems that are important for processing and for the understanding of material properties. The Ca–Co–Zn–O phase diagram consists of two low-dimensional phases, namely, $Ca_3(Co,Zn)_4O_{9-z}$ with misfit layered structure, and $Ca_{n+2}(Co,Zn)_n(Co,Zn)'O_{3n+3-z}$ with one-dimensional cobalt oxide chains that offer interesting thermoelectric properties. The homogeneity ranges of the $Ca_3(Co,Zn)_4O_{9-x}$ and $Ca_{n+2}(Co,Zn)_n(Co,Zn)'O_{3n+3-z}$ solid solutions have been determined. Zn substitution does not have much effect on the thermoelectric properties of the $Ca_3(Co,Zn)_4O_{9-z}$ series. Although the $Ca_{n+2}(Co,Zn)_n(Co,Zn)'O_{3n+3-z}$ oxides exhibit relatively high Seebeck coefficient and low thermal conductivity in general, their resistivity values, however, are relatively high. Although Zn-doping lowers the resistivity of the $Ca_3(Co,Zn)_2O_{6-z}$ series between 300 and 600 K, the Seebeck coefficients, however, also become lower. Unless we can decrease the resistivity of the $Ca_3Co_2O_6$ type phases via proper substitution and improved processing, the best cobaltite materials for thermoelectric applications, at present, remain to have the $Ca_3Co_4O_9$ structure.

Acknowledgments

Use of the Advanced Photon Source at Argonne National Laboratory was supported by the U. S. Department of Energy, Office of Science, Office of Basic Energy Sciences, under Contract no. DE-AC02-06CH11357. One of the authors (SC) would like to thank Dr. J.T. Miller (ANL) and Dr. T. Shibata (IIT) for useful discussions.

References

[1] G.S. Nolas, J. sharp, H.J. Goldsmid, Thermoelectric: Basic Principles and New Materials Developments, Springer, New York, 2001.
[2] T.M. Tritt, M.A. Subramanian, guest editors, Harvesting energy through thermoelectrics: power generation and cooling, MRS Bulletin, Materials Research Society (2006).
[3] T.M. Tritt, Science 272 (1996) 1276.
[4] Kuei Fang Hsu, Sim Loo, Fu Guo, Wei Chen, Jeffrey S. Dyck, Ctirad Uher, Tim Hogan, E.K. Polychroniadis, Mercouri G. Kanatzidis, Science 303 (2004) 818.
[5] R. Venkatasubramanian, E. Siivola, T. Colpitts, B. O'Quinn, Nature 413 (2001) 597.

[6] S. Ghamaty, N.B. Eisner, Proceeding of Interpack 2005: ASME Technical Conference on Packaging of MEMS, NEWS and Electric Systems, July 17–22, 2005, San Francisco, CA.
[7] M.S. Dresselhaus, G. Chen, M.Y. Tang, R.G. Yang, H. Lee, D.Z. Wang, Z.F. Ren, J.P. Fleurial, P. Gogna, Materials Research Society Symposium Proceedings 886, Materials and Technologies for Direct Thermal-to-Electric Energy Conversion, 2006, pp. 3–12.
[8] I. Terasaki, Y. Sasago, K. Uchinokura, Phys. Rev. B 56 (1997) 12685–12687.
[9] M. Mikami, R. Funashashi, M. Yoshimura, Y. Mori, T. Sasaki, J. Appl. Phys. 94 (10) (2003) 6579–6582.
[10] M. Mikami, R. Funahashi, J. Solid State Chem. 178 (2005) 1670–1674.
[11] D. Grebille, S. Lambert, F. Bouree, V. Petricek, J. Appl. Crystallogr. 37 (2004) 823–831.
[12] A.C. Masset, C. Michel, A. Maignan, M. Hervieu, O. Toulemonde, F. Studer, B. Raveau, Phys. Rev. B 62 (2000) 166–175.
[13] H. Minami, K. Itaka, H. Kawaji, Q.J. Wang, H. Koinuma, M. Lippmaa, Appl. Surf. Sci. 197 (2002) 442–447.
[14] Y.F. Hu, W.D. Si, E. Sutter, Q. Li, Appl. Phys. Lett. 86 (2005) 082103.
[15] Powder Diffraction File (PDF), produced by ICDD, Newtown Square, 12 Campus Blvd., Newtown Squares, PA 19073-3273, USA.
[16] J. Wang, B.H. Toby, P.L. Lee, L. Ribaud, S. Antao, C. Kurtz, M. Ramanathan, R.B. Von Dreele, M.A. Beno, Rev. Sci. Instrum. 79 (2008) 085105.
[17] P.L. Lee, D. Shu, M. Ramanathan, C. Preissner, J. Wang, M.A. Beno, R.B. Von Dreele, L. Ribaud, C. Kurtz, S.M. Antao, X. Jiao, B.H. Toby, J. Synchr. Radiat. 15 (2008) 427–432.
[18] C. Preissner, D. Shu, B.H. Toby, P. Lee, J. Wang, D. Kline, K. Goetze, Nucl. Instrum. Meth. Phys. Res. A, in press.
[19] L.R. Dalesio, J.O. Hill, M. Kraimer, S. Lewis, D. Murray, S. Hunt, S.W. Watson, M. Clausen, J. Dalesio, Nucl. Instrum. Meth. Phys. Res. A 352 (1994) 179–184.
[20] Standard reference materials (SRMTM) are produced by National Institute of Standards SRM Office, Gaithersburg, MD 20899. For details, please contact srminfo@nist.gov.
[21] H.M. Rietveld, J Appl. Cryst. 2 (1969) 65–71.
[22] A.C. Larson, R.B. von Dreele, GSAS—General Structure Analysis System, US Government contract (W-7405-ENG-36) by the Los Alamos National laboratory, which is operated by the University of California for the U.S. Department of Energy, 1992.
[23] C.U. Segre, et al., Synchrotron Radiation Instrumentation: Eleventh U.S. Conference CP521, 2000, pp. 419–422.
[24] M. Newville, J. Synchr. Radiat. 8 (2001) 322–326.
[25] B. Ravel, M. Newville, J. Synchr. Radiat 12 (4) (2005) 537–541.
[26] E.R. Segnit, J. Am. Ceram. Soc. 37 (6) (1954) 273–377.
[27] A. Whitaker, D.F. Borton, J. Mater. Sci. 7 (1972) 194–197.
[28] D. Grebille, S. Lambert, F. Bouree, V. Petricek, J. Appl. Crystallogr 37 (2004) 823–831.
[29] A.C. Masset, C. Michel, A. Maignan, M. Hervieu, O. Toulemonde, F. Studer, B. Raveau, Phys. Rev. B 62 (2000) 166–175.
[30] H. Minami, K. Itaka, H. Kawaji, Q.J. Wang, H. Koinuma, M. Lippmaa, Appl. Surf. Sci. 197 (2002) 442–447.
[31] Y.F. Hu, W.D. Si, E. Sutter, Q. Li, Appl. Phys. Lett. 86 (2005) 082103.
[32] E. Woermann, A. Muan, J. Inorg. Chem 32 (1970) 1455.
[33] H. Fjellvag, E. Gulbrandsen, S. Aasland, A. Olsem, B.C. Hauback, J. Solid State Chem. 124 (1996) 190.
[34] W. Wong-Ng, G. Liu, J. Martin, E. Thomas, N. Lowhorn, M. Otani, J. Appl. Phys. 107 (2010) 033508.
[35] T. Takami, H. Ikuta, U. Mizutani, Jpn. J. Appl. Phys. 43 (22) (2004) 8208–8212.
[36] K. Boulahya, M. Parras, J.M. González-Calbet, J. Solid State Chem. 142 (1999) 419–427.
[37] K. Boulahya, M. Parras, J.M. González-Calbet, J. Solid State Chem. 145 (1999) 116–127.
[38] H. McMurdie, M. Morris, E. Evans, B. Paretzkin, W. Wong-Ng, L. Ettinger, C.R. Hubard, Powder Diff. 1 (1988) 76.
[39] W.L. Roth, J. Phys. Chem. Solids 25 (1964) 1.
[40] A. Navrotsky, A. Muan, J. Inorg. Nucl. Chem. 32 (11) (1970) 3471–3484.
[41] K. Krezhov, K. Petrov, T. Karamaneva, J. Solid State Chem. 48 (1983) 33–39.
[42] S. Kawasaki, M. Takano, T. Inami, J. Solid State Chem. 145 (1999) 302–308.
[43] G. Bergerhoff, D.O. Schmitz, Z. Anorg. Allg. Chem. 284 (1956) 10.
[44] C. Tusche, H.L. Meyerheim, J. Kirschner, Phy. Rev. Lett 99 (2007) 026102.
[45] J.Y. Lu, M.A. Lawandy, J. Li, T. Yuen, C.L. Lin, Inorg. Chem. 38 (1999) 2695.
[46] Lampe-önnerud, H.-C. zur Loye, Inorg. Chem. 35 (1996) 2155–2156.
[47] W. Wong-Ng, J.A. Kaduk, G. Liu, Powder Diff. 26 (2011) 22.
[48] M. Mikami, R. Funahashi, IEEE Proceedings on 22nd International Conference on Thermoelectrics, 2003, pp. 200–202.
[49] S. Hébert, D. Flahaut, C. Martin, S. Lemonnier, J. Noudem, C. Goupil, A. Maifnan, J. Hejtmanek, Prog. Solid State Chem 35 (2007) 457–467.
[50] K. Iwasaki, H. Yamane, S. Kubota, J. Takahashi, M. Shimada, J. Alloy. Compd. 358 (2003) 210–215.
[51] Y. Miyazaki, Solid State Ionics 172 (2004) 463–467.
[52] S. Li, R. Funahashi, I. Matsubara, H. Yamada, K. Ueno, S. Sodeoka, Ceram. Int. 27 (2001) 321–324.
[53] S. Li, R. Funahashi, I. Matsubara, H. Yamada, K. Ueno, S. Sodeoka, H. Yamada, Chem. Mater. 12 (2000) 2424–2427.
[54] M. Prevel, O. Perez, J.G. Noudem, Solid State Sci. 9 (2007) 231–235.
[55] T. Takama, H. Ikuta, U. Mizutani, Jpn. J. Appl. Phys. 43 (12) (2004) 8208–8212.